© 2000 European Space Agency (ESA). Reprinted with permission from Proceedings of the AP2000 Millennium Conference on Antennas & Propagation. Davos, Switzerland, 9-14 April 2000, CD-ROM SP-444, paper p1111.pdf.

INTERNAL DUAL-BAND PATCH ANTENNA FOR MOBILE PHONES

Jani Ollikainen, Outi Kivekäs, Anssi Toropainen, and Pertti Vainikainen

Helsinki University of Technology,
Institute of Radio Communications,
Radio Laboratory,
P.O. Box 3000, FIN-02015 HUT, Finland
Email: jol@radio.hut.fi

INTRODUCTION

Development of small antennas for mobile phones has received a lot of attention during the last few years due to size reduction of the handsets, requirements to keep the amount of RF power absorbed by the user below standardized levels regardless of the handset size, and introduction of multimode phones. Single-band and dual-band phones in which the external whip or helix antenna has been replaced by an internal shorted patch antenna (or PIFA) are already in the market. It may be assumed that in the future there will also be a need for internal antennas which operate in several communication systems. In this paper, a multiresonant dual-band internal handset antenna is introduced. The antenna is based on the dual-resonant antenna structure reported in [1]. To our knowledge, this is the first internal handset antenna which covers the E-GSM900 (880 MHz - 960 MHz), GSM1800 (1710 MHz - 1880 MHz), DECT (1880 MHz - 1900 MHz), PCS1900 (1850 MHz - 1990 MHz), and UMTS (1900 MHz - 2170 MHz) frequencies with a return loss $L_{retn} \geq 6$ dB and high radiation efficiency. Previously shorted patch antennas (or PIFAs) with more than one band of operation have been reported e.g. in [2-4]. The dual-band PIFA was introduced in [2]. The idea was extended to multiband PIFAs in [3]. A compact dual-band PIFA with two capacitive feeds was reported in [4].

ANTENNA DESIGN

The studied antenna consists of three shorted patches, one for the lower band and two for the upper band. The lower band patch (parts a-c in Fig. 1) and one of the upper band patches (part d) have been joined together to form a dual-band element having only one short circuit and one feed. This dual-band element has been folded into a meander line -like shape to better fit it into the geometry of a mobile phone. The third shorted patch (part e) is positioned next to the upper band section of the dual-band element to obtain a doubly tuned resonance and a wider impedance bandwidth at the upper band. The dielectric between the patches and the ground plane is air (relative permittivity $\varepsilon_r' = 1$). The antenna is fed by a probe which is connected to the upper band patch of the dual-band element. The total size of the antenna element is 40 mm × 30.4 mm × 7.2 mm (*width* × *length* × *thickness*). It is positioned on top of a ground plane having dimensions 40 mm × 110 mm × 0.3 mm (*width* × *length* × *thickness*). The length and width of the ground plane were selected to be approximately equal to those of the printed circuit board of a typical mobile phone. The antenna structure was designed and theoretically studied using IE3D which is a moment method-based 3D electromagnetic simulation program by Zeland Software.

A prototype antenna was constructed by photoetching the patches, short circuits and the capacitive load from 0.2 mm-thick sheet of tin bronze (contains 96 % copper and 4 % tin, conductivity $\sigma = 1.1 \cdot 10^7$ S/m). The ground plane was made out of 0.3 mm-thick sheet of the same material. The patches are supported above the ground plane by the short circuits, the feed probe, and a 40 mm × 10 mm × 7 mm piece of Styrofoam.

Acknowledgements - The postgraduate studies of the first two authors have been financially supported by the Academy of Finland, Graduate School in Electronics, Telecommunications and Automation (GETA), Jenny and Antti Wihuri Foundation, Nokia Foundation, and Tekniikan Edistämissäätiö. The radiation patterns of the constructed prototype antenna were measured in the anechoic chamber of LK-Products, Finland.

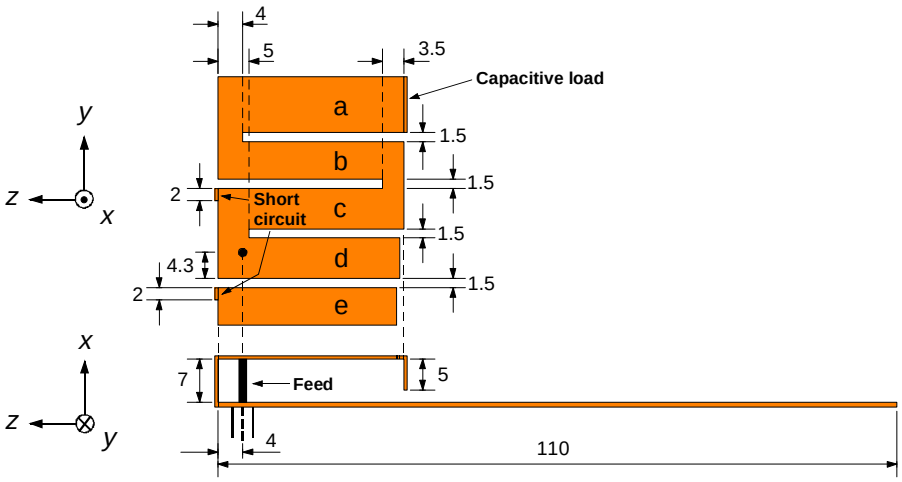

Part	Length (mm)	Width (mm)
a	30	9
b	30	6
c	30	6.5
d	29	6.5
e	28.8	6

Fig. 1. Studied antenna configuration. All dimensions are in millimeters.

RESULTS

The frequency responses of the measured and simulated reflection coefficients are shown in Fig. 2. A good agreement between the simulated and measured results can be observed. The measured impedance bandwidth ($L_{retn} \geq 6$ dB) of the lowest band is 12.4 % (115 MHz) at the center frequency f_c = 926 MHz. For the dual-resonant upper band, the measured bandwidth ($L_{retn} \geq 6$ dB) is 27.7 % (535 MHz) at f_c = 1934 MHz. Above the desired bands, there is also a third band with the bandwidth of 3.6 % (89 MHz) at f_c = 2515 MHz. The third band is assumed to be caused by the $3\lambda/4$-resonance of the lower band section of the meandered antenna element. This resonance has been tuned down from 2700 MHz by the presence of the upper band section of the meandered dual-band element (part d in Fig.1). According to simulations, the impedance bandwidth of the antenna depends on the length of the ground plane. However, in this design the ground plane length is not optimized with respect to the bandwidth.

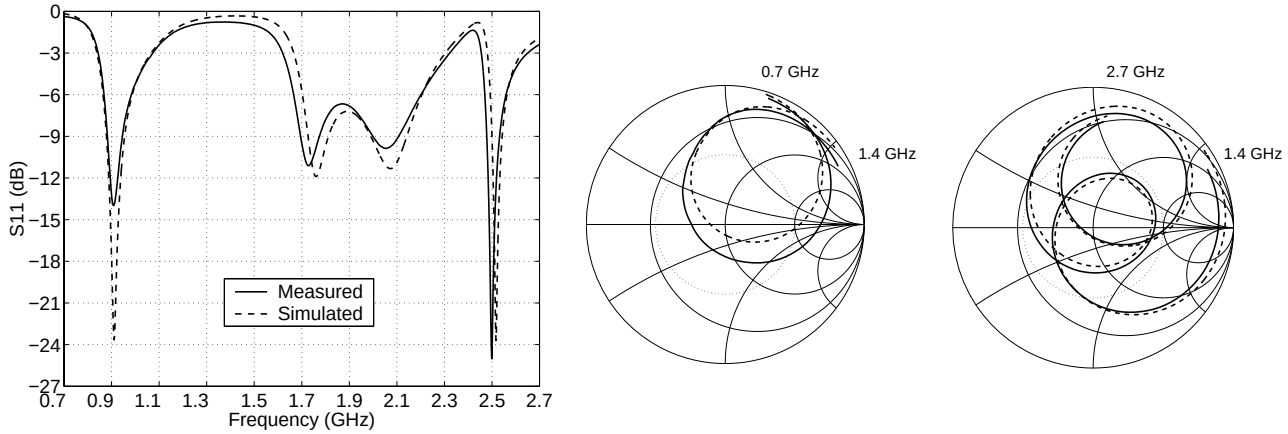

Fig. 2. Measured (solid line) and simulated (dashed line) reflection coefficient as a function of frequency. Dotted circles on the Smith charts represent L_{retn} = 6 dB.

The measured and simulated cuts of the radiation patterns of the studied antenna are shown in Fig. 3. The presented cuts have been obtained in free space. At 920 MHz, the radiation pattern is almost omnidirectional and resembles that of a half-wave dipole. At 1710 MHz, the pattern becomes more complex and somewhat more directive. The directivity increases with frequency. At the same time the pattern maximum tilts towards the negative *z*-axis. In addition, it can be seen in Fig. 3 that the polarization of the antenna at the lower band is different from the polarization at the upper band.

Fig. 4. shows the simulated radiation efficiency (IE3D) of the antenna in free space. The conductivity used in the calculations was $\sigma = 1.1 \cdot 10^7$ S/m. The efficiency stays above 95 % over the two desired bands of operation.

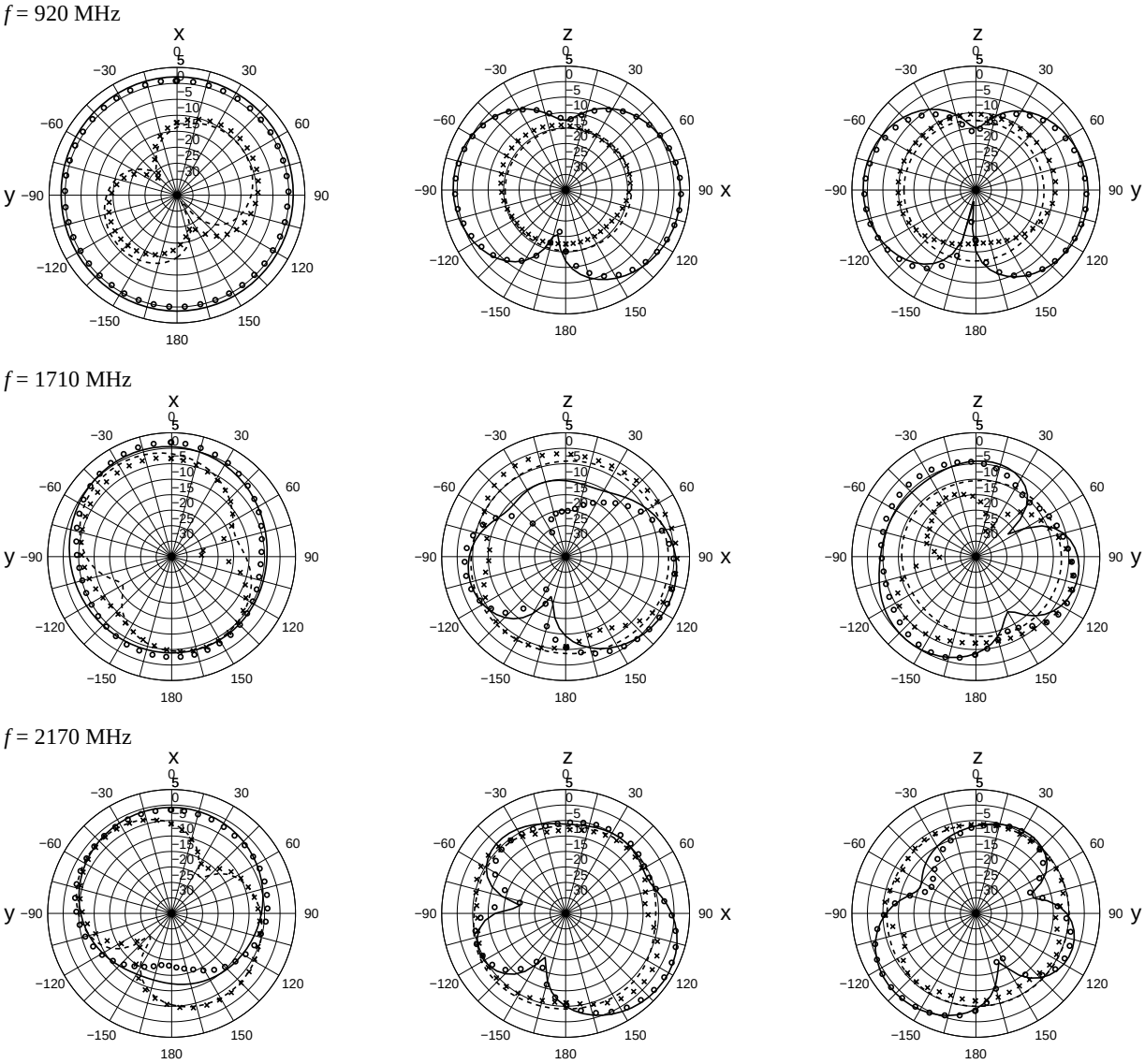

Fig. 3. Measured (o o o E_θ , x x x E_φ) and simulated (—— E_θ , – – – E_φ) cuts of the radiation patterns at 920 MHz, 1710 MHz, and 2170 MHz. Antenna orientation is given in Fig. 1. Results include the effect of mismatch loss. Radial unit is dBi.

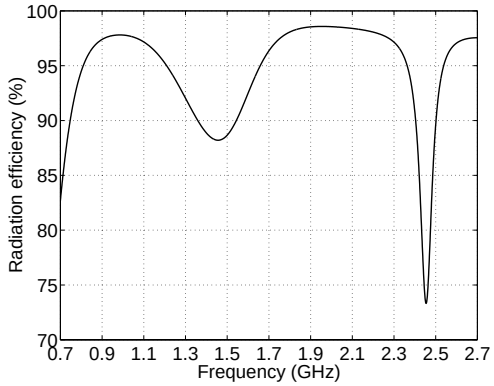

Fig. 4. Simulated (IE3D) radiation efficiency in free space as a function of frequency for the studied antenna. Conductivity of metal parts $\sigma = 1.1 \cdot 10^7$ S/m.

The specific absorption rate (*SAR*) characteristics of the studied antenna were evaluated by simulations which were performed using a commercial FDTD program (XFDTD, version 5.0 Bio-Pro by Remcom, Inc.). An FDTD mesh of a male head and shoulders with the voxel resolution of 2.5 mm was used. This was based on the standard human head and shoulders mesh (3 mm voxel) obtained from Remcom. The values of the tissue parameters (ε_r', σ_{eff}) were interpolated from the values given in [5]. The tissue density values were those provided with the original mesh. The phone model (antenna and thin ground plane) was placed beside the head model according to the intended use position specified by CENELEC [6]. This was obtained by rotating the head model forward by 74° and to the right by 10° while keeping the phone model vertical in the mesh. The distance of 11.9 mm (5 cells) was left between the head and phone model. The *SAR*s were calculated at 915 MHz, 1730 MHz, and 2100 MHz using a steady-state sinusoidal excitation. Due to the limitations of the 2.5 mm grid, the dimensions of the antenna, and thus also its resonant frequencies, were slightly different from those of the measured antenna. The frequencies used in *SAR* simulations were adjusted accordingly. The simulation space enclosing the head and the handset consisted of 207 × 187 × 206 cells. The simulations were run for 4000 timesteps to ensure converged results.

The results of the *SAR* simulations are listed in Table 1. The maximum 10 g average *SAR* value was located near the center of the ground plane at 915 MHz. At 1730 MHz, the maximum was found near the short circuit of the parasitic resonator (part e in Fig. 1), and at 2100 MHz near the short circuit of the meandered patch. The results indicate that the *SAR*s are below the basic restrictions set by CENELEC. When studying the *SAR* values given in Table 1, it must be noted that the specified mean (rms) output powers for handsets in GSM900, GSM1800, DECT, and UMTS systems are 250 mW, 125 mW, 10 mW, and 250 mW, respectively. The radiation efficiencies when the phone model is beside the head are also listed in Table 1. The radiation efficiencies at 1730 MHz and 2100 MHz are more than twice as high as the efficiency at 915 MHz. This is partly explained by more directive radiation patterns at 1730 MHz and 2100 MHz.

Table 1. Simulated maximum 10 g average *SAR* values in the head, and simulated radiation efficiencies (XFDTD) with prototype beside the head. *SAR* results are normalized to 1 W of CW input power.

f (MHz)	915	1730	2100
Max 10 g average *SAR* (W/kg)	4.6	1.8	1.8
Radiation efficiency (%)	29	72	75

CONCLUSIONS

A multiresonant internal dual-band shorted patch antenna for mobile phones has been studied. Both simulated and measured results have been presented. The studied antenna has two bands of operation, the lower one ranges from 868 MHz to 983 MHz (12.4 %) and the upper one from 1666 MHz to 2201 MHz (27.7 %). The radiation patterns are suitable for internal handset antenna application. According to simulated results with FDTD, the *SAR* values caused by the antenna are below the limits set by CENELEC.

REFERENCES

[1] J. Ollikainen and P. Vainikainen, "Radiation and bandwidth characteristics of two planar multistrip antennas for mobile communication systems," *Proc. IEEE 48th Vehicular Technology Conference*, Vol. II, Ottawa, Ontario, Canada, May 18-21, 1998, pp. 1186-1190.

[2] Z. D. Liu, P. S. Hall, and D. Wake, "Dual-frequency planar inverted-F antenna", *IEEE Transactions on Antennas and Propagation*, Vol. 45, No. 10, October 1997, pp. 1451-1458.

[3] P. Song, P.S. Hall, H. Ghafouri-Shiraz, and D. Wake, "Triple-band planar inverted-F antenna", *IEEE Antennas and Propagation International Symposium Digest*, Vol. 2, Orlando, Florida, July 11-16, 1999, pp. 908-911.

[4] C. R. Rowell and R. D. Murch, "A compact PIFA suitable for dual-frequency 900/1800-MHz operation", *IEEE Transactions on Antennas and Propagation*, Vol. 46. No. 4, April 1998, pp. 596-598.

[5] *User's Manual for XFDTD the Finite Difference Time Domain Graphical User Interface for Electromagnetic Calculations*, Version 5.04, Remcom, Inc., February 1999, 128 p.

[6] European specification (ES 59005), *Considerations for the Evaluation of Human Exposure to Electromagnetic Fields (EMFs) from Mobile Telecommunication Equipment (MTE) in the Frequency Range 30 MHz - 6 GHz*, Brussels, Belgium, CENELEC, October 1998, 81 p.